energies

MDPI

Article

Multi-Model-Based Predictive Control for Divisional Regulation in the Direct Air-Cooling Condenser

Zhiling Luo [1,*] and Qi Yao [2]

[1] School of Control and Computer Engineering, North China Electric Power University, Beijing 102206, China
[2] Energy and Electricity Research Center, Jinan University, Zhuhai 519070, China; qiyao@jnu.edu.cn
* Correspondence: aloha.l@163.com

Abstract: Flow distortions caused by ambient wind can have complex negative effects on the performance of direct air-cooling condensers, which use air as their cooling medium. A control-oriented model of the direct air-cooling condenser model, considering fan volumetric effectiveness and plume recirculation rate, was developed, and its linearization model was derived. The influences of fan volumetric effectiveness and plume recirculation rate on backpressure were analyzed, and the optimal backpressure was calculated. To improve both the transient performance and steady-state energy saving of the condenser, a multi-model-based predictive control strategy was proposed to divisionally adjust the fan array. Four division schemes of the direct air-cooling fan array constituted the local models, and in each division scheme, axial fans were divided into three groups according to the wind direction: windward fans, leeward fans, and other fans. The simulation results showed that the turbine backpressure can be increased by 15 kPa under the influence of plume recirculation and the reduction of the fan volumetric efficiency. The fan division adjustment strategy can achieve satisfactory control performance with switching rules.

Keywords: backpressure; direct air-cooling condenser; divisional regulation; multi-model; plume recirculation

Citation: Luo, Z.; Yao, Q. Multi-Model-Based Predictive Control for Divisional Regulation in the Direct Air-Cooling Condenser. *Energies* **2022**, *15*, 4803. https://doi.org/10.3390/en15134803

Academic Editor: Pawel Madejski

Received: 17 May 2022
Accepted: 27 June 2022
Published: 30 June 2022

1. Introduction

Direct air-cooling condensers are widely used in coal-fired and concentrated solar power plants because of their water-saving advantages [1]. As the specific heat capacity of air is smaller than that of water, the heat exchange efficiency is reduced, resulting in a significantly higher pressure in the direct air-cooling condenser than in the water-cooled condenser, which leads to a reduction in the turbine power output [2,3]. To improve system efficiency, it is important to understand the direct air-cooling condenser performance and study the relationship between condenser pressure and related variables.

Installed on an outdoor platform with a height of tens of meters, the performance of the direct air-cooling condenser is affected by factors such as turbine steam load ratio, fan speed, ambient temperature, wind speed, wind direction, and windscreens [4–7]. Flow distortion or disturbance caused by wind can negatively impact the performance of the condenser, resulting in complex fluctuations in fan inlet flow and temperature. Volumetric effectiveness and plume recirculation rate are used to evaluate the effect of the fan inlet flow and temperature fluctuations on direct air-cooling condenser performance, respectively. The crosswinds significantly reduce the volumetric effectiveness of windward fans, while winds along with the longitudinal lead to the increase in plume recirculation [8].

Fan volumetric effectiveness is defined as the ratio of the airflow through the fan with inlet disturbance to the airflow of the fan operating independently and without inlet disturbance, which is also called cluster factor in recent studies. Through scaled-down model experiments, Salta [9] found that the fan volumetric effectiveness of peripheral fans was always lower than that of internal fans, and presented the relationship between fan volumetric effectiveness and platform height, fan diameter, and walkway width. Fourie [10] derived

the correlation between fan volumetric effectiveness and crosswind speed. Through CFD simulation, Yang [11] presented that the aerodynamic characteristics of axial fans located at different positions of the fan array had different performances: the volumetric effectiveness of windward fans was lower than that of internal fans under the crosswind, while the volumetric effectiveness of leeward fans was higher, and the volumetric effectiveness value was affected by wind speed and direction.

Plume recirculation occurs when a part of the hot plume exiting the direct air-cooling condenser returns into the fan inlet [8]. The plume recirculation rate fluctuates with the wind direction and is relatively high when the wind direction is from the boiler direction, because the air temperature from the direction of the boiler is warmer, which reduces the heat exchange efficiency of the condenser. In operation, there have been cases of emergency shutdowns of power plants due to a crosswind in the direction of the boiler. Louw simulated the effects of various wind speeds and directions on a large air-cooling condenser with 386 air-cooling units and concluded that windward fans had the worst performance, and the edge fans were affected by plume recirculation [12].

In the research of modeling and optimization of the direct air-cooling condenser, numerical simulation and experimental research are the main methods. There are few studies about the development of control-oriented models, which have significant effects on improving power plant efficiency. Guo [13] established a dynamic model of the air-cooling condenser, analyzed the influence of fan face velocity and ambient temperature on back-pressure, and applied it to the primary frequency regulation of a grid. Yang [14] combined the backpressure regulation of the direct air-cooling condenser with the boiler-turbine coordinated control system and achieved backpressure optimization and an accelerated turbine load response by controlling the fan speed. Zhang [15] developed a direct air-cooling condenser model based on the moving-boundary method and adopted feedforward compensation to suppress the backpressure disturbance caused by the ambient temperature variation. This model considered fan volumetric effectiveness but did not show its relationship to backpressure. None of these dynamic models reflected the negative effects of plume circulation.

In control-oriented modeling, the direct air-cooling system is usually simplified as one air-cooling module or one finned tube, and dozens of fans are regarded as a whole, which is adjusted uniformly. Studies on the performance of direct air-cooling condensers have suggested the necessity of fan divisional control to improve system efficiency. Liu [16] calculated the influence of operating conditions, fan speeds, and environmental parameters on the backpressure and coal consumption of direct air-cooling power plants through grey correlation analysis, which can be a reference for fan array divisional regulation. Li [17] simulated the flow field and temperature field of the direct air-cooling condenser, calculated the correlation between the rotational speed of each fan and the condenser pressure, and suggested adjusting the fans with a relatively higher correlation with condenser pressure is beneficial to reducing condenser pressure and improving efficiency. Huang [18,19] calculated optimal fan speed adjustment strategies under different meteorological conditions and proposed adjusting the fan speed in different blocks under different wind directions. Through scale-down experiments, we found that fan array divisional regulation can help save about 13% of fan energy consumption [20]. However, it is difficult to estimate model parameters and implement a control system, because few power plants are equipped with measurement points for volumetric effectiveness and plume recirculation rate systems. To overcome the problem of no measurement points, we designed a multi-model predictive control system that switched based on local model errors.

The contribution of this paper is to develop a dynamic direct air-cooling condenser model and propose a multi-model-based predictive control strategy for backpressure regulation. The novelties of this paper include: (1) establishing a control-oriented direct air-cooling condenser model, which considers volumetric effectiveness and the plume recirculation rate, and derives its linearization model; (2) the effects of volumetric effectiveness and plume recirculation rate on the dynamic response time and static gain of backpressure under various operating

conditions are demonstrated; (3) the local model of the direct air-cooling condenser adopts fan divisional regulation schemes that change with the wind direction; (4) a model switching signal is designed to realize the switching of various fan divisional regulation schemes. The rest of this paper is organized as follows: Section 2 introduces the structure and the layout of the direct air-cooling condenser. Section 3 establishes and linearizes a dynamic model of an air-cooling unit of the condenser, validates the model, and analyzes the performance of the model. In Section 4, a multi-model predictive control strategy is proposed, and simulations are demonstrated. Finally, conclusions are drawn in Section 5.

2. Description of the System

The investigated 330 MW coal-fired power plant direct air-cooling condenser, located in Hebei Province, China, consists of 30 cooling units in five rows and six columns, arranged in an array shape. As shown in Figure 1, each cooling unit consists of an axial flow fan and hundreds of finned tube bundles. The finned tube bundles form an A-shaped structure. The exhaust steam from the turbine is sent to the finned tube bundles of the outdoor direct air-cooling condenser through the pipe. The cold air in the environment driven by the axial fan flows through the outer surface of the finned tubes and exchanges heat with the steam in order to condense the turbine exhaust steam into water. Part of the hot air leaving the air-cooling unit returns to the fan inlet under the influence of flow distortion and the ambient wind, which is called plume recirculation. The condensed water returns to the heat recovery system through the condensate pump. The pressure of the condenser is a key parameter that affects the power output of the coal-fired power plant. It needs to be optimized and regulated to a certain range. The designed parameters of the condenser are presented in Table 1.

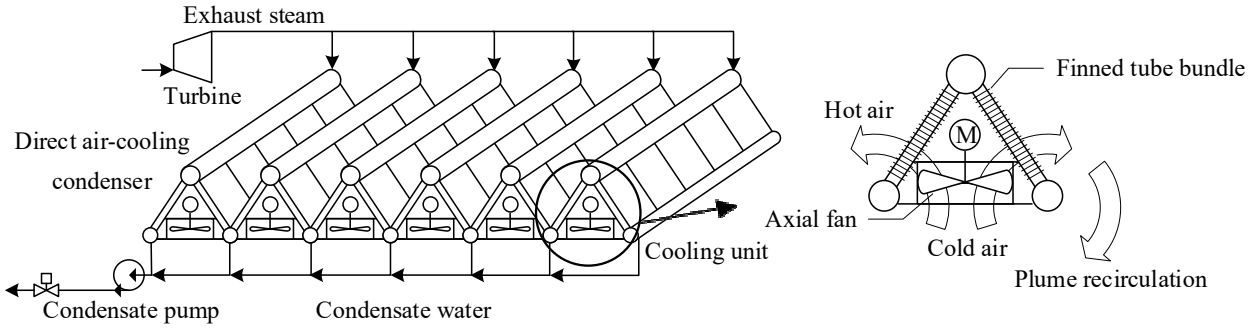

Figure 1. The schematic of the cold-end system.

Table 1. The Designed Parameters of the Direct Air-Cooling Condenser.

Parameter (Unit)	Value
Power plant nominal power (MW)	330
Exhaust steam mass flow rate (t/h)	741
Exhaust steam enthalpy (kJ/kg)	2531
Backpressure (kPa)	15
Ambient temperature (°C)	15
Fan rotational speed (r/min)	100
Fan nominal power (kW)	110
Fan front face area (m^2)	211
Fan face velocity (m/s)	2.46
Finned tube number of each cooling unit (-)	370
Finned tube length (m)	10.4
Finned tube mass (kg)	15.2
Finned tube combined specific heat capacity (kJ/(kg·K))	2.72
Finned tube wall density (kg/m^3)	7850
Finned tube cross-section area (m^2)	0.0033
Finned tube inner surface area (m^2)	2.06
Finned tube outer surface area (m2)	61.9
Finned tube inner surface heat transfer coefficient ($W/(m^2 \cdot K)$)	7200
Finned tube outer surface heat transfer coefficient ($W/(m^2 \cdot K)$)	35

Under the complex influence of ambient wind, the heat exchange efficiency of the air-cooling units located in different positions of the direct air-cooling condenser is significantly different. Figure 2 is the planer layout of the investigated coal-fired power plant, including the distribution of the direct air-cooling condenser, turbine house, and boiler house. Every circle represents a cooling unit. The local prevailing wind direction is 330°. The figure also shows the windward and leeward fans when the wind direction is 270°. The winds in the directions of 0° and 90° are crosswind, which significantly reduces the volumetric effectiveness of windward fans. The winds in the directions of 180° and 270° are longitudinal wind, which mainly leads to the increase in plume recirculation. The boiler is set in the downwind direction to avoid the effect of the warm crosswind in the direction of the boiler on the condenser.

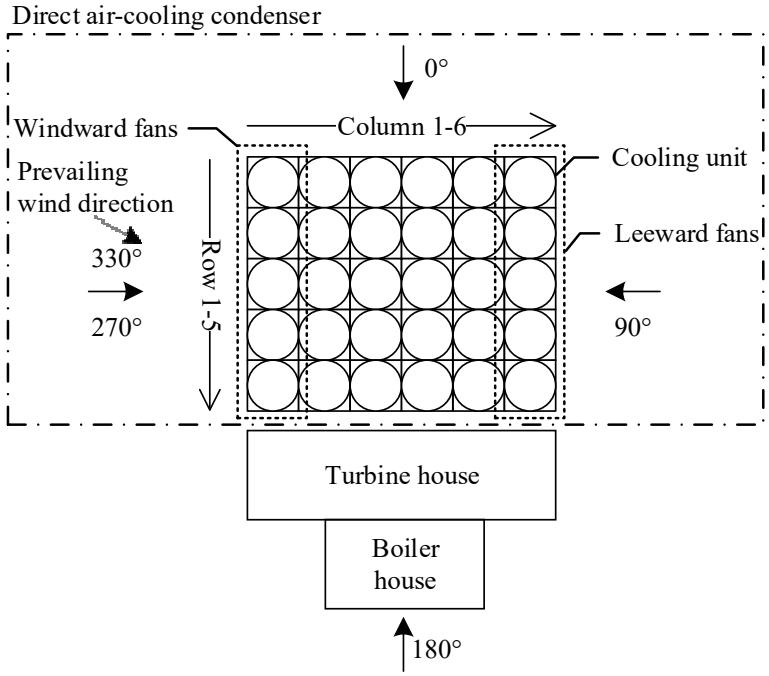

Figure 2. The planar layout of a direct air-cooling generating unit.

3. Model Development

This section presents the process model of an air-cooling unit, describing the dynamic effects of volumetric effectiveness, plume recirculation, and fan speed on the condenser, and the model is linearized and validated for control. Based on the air-cooling unit model established by Zhang [15], this paper originally describes the plume recirculation of the air-cooling unit and the derivation of the model linearization.

3.1. Process Model Development

With the conservation of energy and mass, the air-cooling unit can be described by a lumped parameter model with the moving-boundary approach [15].

The assumptions utilized in the derivation of the model include [21]: (1) the air-cooling unit is simplified into a long and thin horizontal tube; (2) there is only a two-phase region in the air-cooling unit; (3) the steam flows through the tube one-dimensionally; (4) the axial heat conduction and pressure drop are negligible. The schematic of the air-cooling unit model is shown in Figure 3.

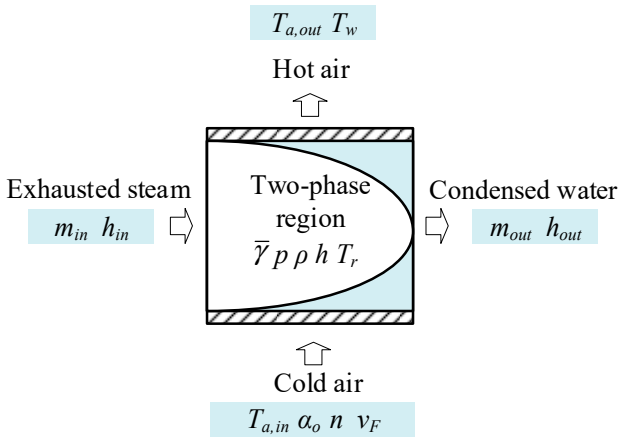

Figure 3. A schematic of the simplified air-cooling unit model.

1. Conservation of steam mass and energy

Mass conservation:

$$A_s L \frac{d\rho}{dt} = \dot{m}_{in} - \dot{m}_{out} \tag{1}$$

where ρ is the average density in the two-phase region; $\dot{m}$ is the steam mass flow rate; the subscript *in* and *out* represent the inlet and outlet of the condenser, respectively; A_s and L are the cross-section area and length of the finned tube, respectively.

Energy conservation:

$$A_s L \left(\frac{d\rho h}{dt} - \frac{dp}{dt} \right) = \dot{m}_{in} h_{in} - \dot{m}_{out} h_{out} + \alpha_i A_i (T_w - T_r) \tag{2}$$

where h and p are the enthalpy and condenser pressure in the two-phase region, respectively; α_i and A_i are the heat transfer coefficient and area of the inner surface of the finned tubes, respectively; T is temperature; the subscript w and r represent the finned tube wall and steam, respectively.

The density and enthalpy of the two-phase region are calculated as follows:

$$\rho = \bar{\gamma}\rho_g + (1 - \bar{\gamma})\rho_l \tag{3}$$

$$h = \frac{\bar{\gamma}\rho_g h_g + (1 - \bar{\gamma})\rho_l h_l}{\bar{\gamma}\rho_g + (1 - \bar{\gamma})\rho_l} \tag{4}$$

The subscript l and g are liquid and gas, respectively; $\bar{\gamma}$ is the two-phase mean void fraction, defined as the ratio of gas volume to two-phase region volume, which can be determined as [21]:

$$\bar{\gamma} = \frac{c}{(x_{out} - x_{in})(c-1)^2} \ln \left[\frac{x_{in}(c-1) - c}{x_{out}(c-1) - c} \right] - \frac{1}{c-1} \tag{5}$$

where $c = (\rho_g/\rho_l)^{2/3}$, x is the steam dryness, and the subscript *in* and *out* represent the inlet and outlet of the condenser, respectively.

By differentiating the variables, Equations (1), (2) and (5) can be expressed as:

$$A_s L \left[\frac{d\rho_l}{dp}(1 - \bar{\gamma}) + \frac{d\rho_g}{dp}\bar{\gamma} \right] \frac{dp}{dt} + A_s L (\rho_g - \rho_l) \frac{d\bar{\gamma}}{dt} = \dot{m}_{in} - \dot{m}_{out} \tag{6}$$

$$A_s L \left[\frac{d\rho_l h_l}{dp}(1 - \bar{\gamma}) + \frac{d\rho_g h_g}{dp}\bar{\gamma} - 1 \right] \frac{dp}{dt} + A_s L (\rho_g h_g - \rho_l h_l) \frac{d\bar{\gamma}}{dt} = \dot{m}_{in} h_{in} - \dot{m}_{out} h_{out} + \alpha_i A_i (T_w - T_r) \tag{7}$$

$$\frac{d\bar{\gamma}}{dt} = \frac{\partial\bar{\gamma}}{\partial p}\frac{dp}{dt} + \frac{\partial\bar{\gamma}}{\partial x_{in}}\left(\frac{\partial x_{in}}{\partial p}\frac{dp}{dt} + \frac{\partial x_{in}}{\partial h_{in}}\frac{dh_{in}}{dt}\right) + \frac{\partial\bar{\gamma}}{\partial x_{out}}\left(\frac{\partial x_{out}}{\partial p}\frac{dp}{dt} + \frac{\partial x_{out}}{\partial h_{out}}\frac{dh_{out}}{dt}\right) \quad (8)$$

2. Conservation of finned tube wall energy

$$C_{p,w}m_w\frac{dT_w}{dt} = \alpha_i A_i(T_r - T_w) + \alpha_o A_o(T_{a,in} - T_w) \quad (9)$$

where $C_{p,w}$ is the finned tube's combined specific heat capacity, which is calculated from the specific heat capacity of the fins and the tube wall [15]; m_w is the finned tube's mass; α_o and A_o are the heat transfer coefficient and area of the outer surface of the finned tube, respectively; T_a is air temperature; the subscripts *in* represents the inlet of the axial fan.

3. Conservation of air energy

$$C_{p,a}\rho_a v_F A_F(T_{a,in} - T_{a,out}) = \alpha_o A_o(T_{a,in} - T_w) \quad (10)$$

where $C_{p,a}$ and ρ_a are specific heat capacity and air density, respectively; v_F and A_F are face velocity and the front face area of the fan, respectively; $T_{a,out}$ is the air temperature of the fan outlet.

4. Air plume recirculation

The plume recirculation rate, which evaluates the proportion of air leaving the fan that returns to the fan inlet, is defined as [8]:

$$R = \frac{T_{a,in} - T_{a,e}}{T_{a,out} - T_{a,e}} \quad (11)$$

where $T_{a,e}$ is the air temperature of the environment. Combining (10) and (11), eliminating $T_{a,out}$, the relationship between $T_{a,in}$ and $T_{a,e}$ can be obtained:

$$T_{a,in} = \frac{(1-R)C_{p,a}\rho_a v_F A_F T_{a,e} + R\alpha_o A_o T_w}{(1-R)C_{p,a}\rho_a v_F A_F + R\alpha_o A_o} \quad (12)$$

5. Heat transfer coefficient

The heat transfer coefficient inside the finned tube is calculated with laminar condensation correlation [2]:

$$\alpha_i = 1.13\left(\frac{g\sin\varphi\rho^2\lambda^3\phi}{\mu(T_r - T_w)L}\right)^{\frac{1}{4}} \quad (13)$$

where Reynolds number $Re < 1600$, g is gravity acceleration, φ is the angle of the A-frame configuration, λ is the thermal conductivity, φ is wall heat flux density, and μ is the dynamic viscosity of the fluid.

The heat transfer coefficient outside the finned tube can be calculated with the following forced convection heat transfer correlation [2]:

$$\alpha_o = 0.19\frac{\lambda}{d_H}Re^{0.6} \quad (14)$$

where d_H is the hydraulic diameter, $Re = u_{max}d_H/\upsilon$ is the Reynolds number, $2 \times 10^3 < Re < 1.5 \times 10^4$, u_{max} is the airflow rate at the narrowest cross-section, and υ is the kinematic viscosity of the air, which depends mainly on the temperature.

In a variable condition, an empirical formula can be used to calculate the heat transfer coefficient outside the finned tube [2]:

$$\alpha_o = \alpha_{o,0}\left(\frac{v_F\upsilon_0}{v_{F,0}\upsilon}\right)^{0.6} \quad (15)$$

where the subscript 0 represents the designed condition.

6. Axial fan

According to the fan similarity laws, axial fans have the following relationships between volumetric flow rate and power consumption:

$$\frac{V_F}{V_{F,0}} = \frac{n}{n_0} \tag{16}$$

$$\frac{E_F}{E_{F,0}} = \left(\frac{n}{n_0}\right)^3 \tag{17}$$

where V_F is the fan volumetric flow rate, E_F is the power consumption of an axial fan, n is the fan speed, and subscript 0 represents the nominal value.

Fan volumetric effectiveness, defined as the ratio of the actual airflow through the fan to that of the same fan operating without inlet disturbance, can be expressed as [9]:

$$\eta_F = \frac{V_{F,ac}}{V_F} \tag{18}$$

where $V_{F,ac}$ is the actual air flow rate of the fan. The fan face velocity can be calculated by:

$$v_F = \frac{V_{F,ac}}{A_F} \tag{19}$$

7. Exhaust steam mass flow and enthalpy

The exhaust steam mass flow rate can be calculated by:

$$\dot{m}_{in} = D_0 - \sum D_i \tag{20}$$

where D_0 is the main steam mass flow rate, and D_i is the steam mass flow rate from the ith extraction stage. Statistics show that the exhaust steam mass flow rate is proportional to the turbine steam load ratio β. Therefore, the exhaust steam mass flow rate can be obtained by polynomial fitting with the data provided by the manufacturer, and the expression is $\dot{m}_{in} = 634.1\beta + 52.44$.

Because turbine exhaust steam is wet and dryness is difficult to measure, and the expansion process of steam in the turbine is considered to be an isentropic expansion process, the interstage efficiency model is used to calculate the exhaust enthalpy.

$$h_{in} = h_j - \eta_T(h_j - \widetilde{h}_{in}) \tag{21}$$

where h_j is the last extraction steam enthalpy, η_T is the turbine isentropic efficiency, and $\widetilde{h}_{in}$ is the ideal enthalpy of the exhaust steam. The turbine isentropic efficiency is a function of the pressure ratio between the exhaust steam and last extraction steam, which can be expressed as a quadratic polynomial. The theoretical specific enthalpy of the exhaust steam can be obtained with the known exhaust steam pressure and last extraction steam theoretical entropy.

8. Governing equations

Combining the governing Equations (6)–(9) into a matrix form results in:

$$\dot{x} = D^{-1} f(x, u) \tag{22}$$

with state variables $x = [\ p\ \bar{\gamma}\ h_{out}\ T_w]^T$ and the manipulated variables $u = [m_{in}\ h_{in}\ T_{a,e}\ n]^T$, where

$$D = \begin{bmatrix} d_{11} & d_{12} & 0 & 0 \\ d_{21} & d_{22} & 0 & 0 \\ 0 & 0 & 0 & d_{34} \\ d_{41} & d_{42} & d_{43} & 0 \end{bmatrix}, \; f = \begin{bmatrix} \dot{m}_{in} - \dot{m}_{out} \\ \dot{m}_{in}h_{in} - \dot{m}_{out}h_{out} + \alpha_i A_i (T_w - T_r) \\ \alpha_i A_i (T_r - T_w) + \alpha_o A_o (T_{a,in} - T_w) \\ -\frac{\partial \bar{\gamma}}{\partial x_{in}} \frac{\partial x_{in}}{\partial h_{in}} \frac{dh_{in}}{dt} \end{bmatrix}.$$

The elements in matrix D are given in Appendix A.

The linearized model of the direct air-cooling condenser can be used to investigate the dynamic behavior at an operating point (x_0, u_0). Hence, the model of the direct air-cooling condenser can be linearized as follows:

$$\Delta \dot{x} = A\Delta x + B\Delta u \tag{23}$$

where $A = [D|_{(x_0,u_0)}]^{-1} \frac{\partial f(x,u)}{\partial x}\Big|_{(x_0,u_0)}$, $B = [D|_{(x_0,u_0)}]^{-1} \frac{\partial f(x,u)}{\partial u}\Big|_{(x_0,u_0)}$, and the elements in matrix A and B are given in Appendix A.

3.2. Optimum Condenser Pressure

Turbine backpressure is a parameter that affects the operating economy of the power plant, because when the backpressure increases, the generating power output decreases. The regulation of the axial fan speed is the main way to adjust the backpressure. However, increasing the fan speed to reduce the backpressure is not an ideal operation strategy, since the energy consumed by the axial fans cannot be ignored. When the difference between the turbine power output and the axial fan power is the largest, the fan speed and the corresponding backpressure are optimal. Therefore, this optimization problem is formulated with the following fitness function:

$$max\ \Delta E = E_T - E_F \tag{24}$$

where ΔE is the net power, and E_T is the turbine power output.

According to the relationship between the relative deviation of the turbine power output and the backpressure provided by the manufacturer, the turbine power output under operating conditions can be calculated as [14]:

$$E_T = E_{T,0}\beta(1 + \zeta) \tag{25}$$

where $E_{T,0}$ is the nominal turbine power output, β is the turbine steam load ratio, ζ is the turbine power relative deviation, $\zeta = f(\beta)(p - p_0)$, and $f(\beta) = 0.0034\beta - 0.0064$ is the slope of the backpressure–turbine power increment curve, obtained by polynomial fitting with data provided by the manufacturer.

3.3. Model Validation

The dynamic and linearized models were validated with a fan speed step test of the investigated direct air-cooling condenser of the 330 MW power plant. Before the step test, the fan inlet temperature and face velocity of an edge fan and an internal fan were measured, and the average plume recirculation and fan volumetric effectiveness were calculated. In the step test, the rotation speeds of all fans were adjusted simultaneously. First, the fan rotation speeds were changed from 66 r/min to 44 r/min at t = 15 s, and then from 44 r/min to 65 r/min at t = 500 s. Figure 4 shows the experimental and simulation results of backpressure variation caused by step changes in fan speed. Comparing the four curves, the established model showed a similar dynamic response and steady-state to the actual system. The root mean square error (RMSE) of the nonlinear model was 0.11 kPa, and the RMSE of the linearized model was 0.22 kPa, when R = 0.02 and η = 0.85. When R = 0 and η = 1, the RMSE of the nonlinear model was 1.17 kPa, which indicated that the calculated backpressure is lower than the actual value when the plume recirculation and the fan volumetric effectiveness are not considered.

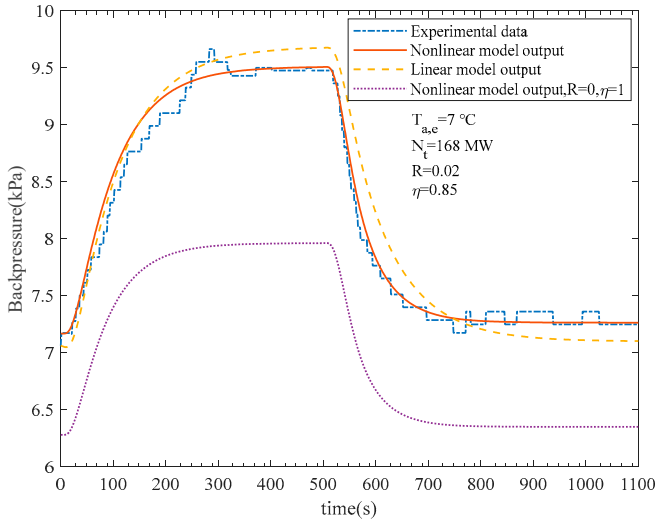

Figure 4. Experimental and simulation results of fan speed step test.

3.4. Model Performance Analysis

1. Step test response

Figure 5 shows the backpressure response at different fan volumetric effectiveness and plume recirculation rates when the fan speed was reduced by 10 r/min under nominal operating conditions. When the operating conditions were unchanged, the condenser performance was significantly affected by the ambient wind. The fan volumetric effectiveness and plume recirculation rate affected both the dynamic response time and static gain of backpressure, and the plume recirculation rate has a particularly significant effect on the static gain of backpressure.

2. Steady-state performance

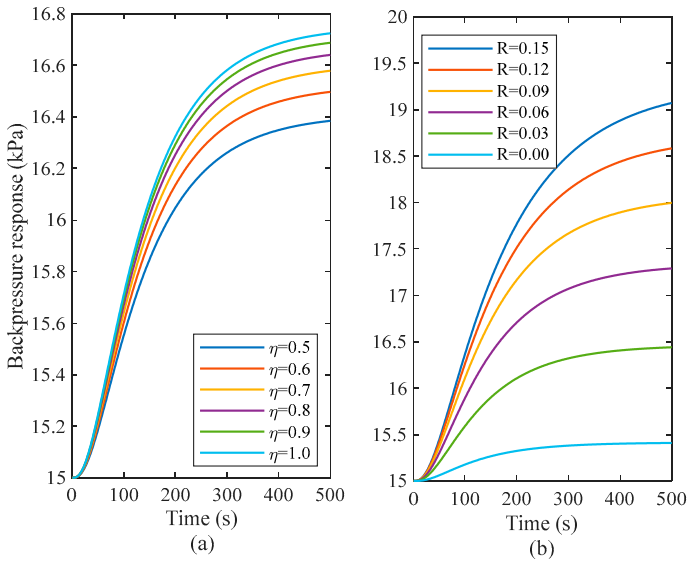

Figure 5. Response of backpressure to fan speed step test: (**a**) backpressure at different fan volumetric effectiveness; (**b**) backpressure at different plume recirculation rates.

Figures 6–8 show the steady-state performance of the direct air-cooling condenser model under different operating conditions. Figures 6 and 7 show that the backpressure increased with increasing ambient temperature and an increasing turbine steam load ratio, and with decreasing fan rotational speed, which is consistent with the model performance

in the literature. The influence of ambient temperature on backpressure is significant, and adjusting the fan speed is an effective way to regulate backpressure.

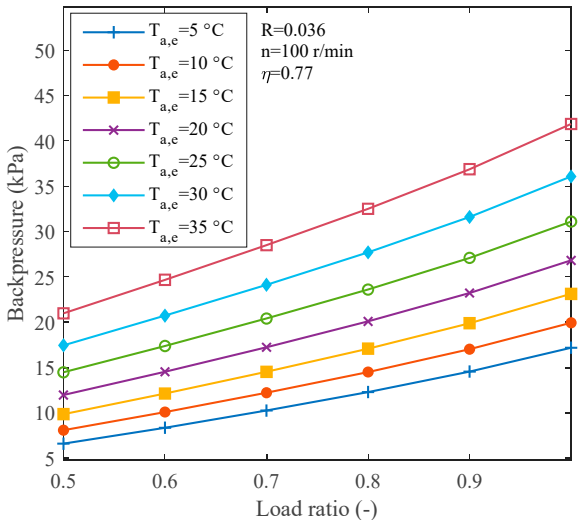

Figure 6. Backpressure at different ambient temperatures and load ratios.

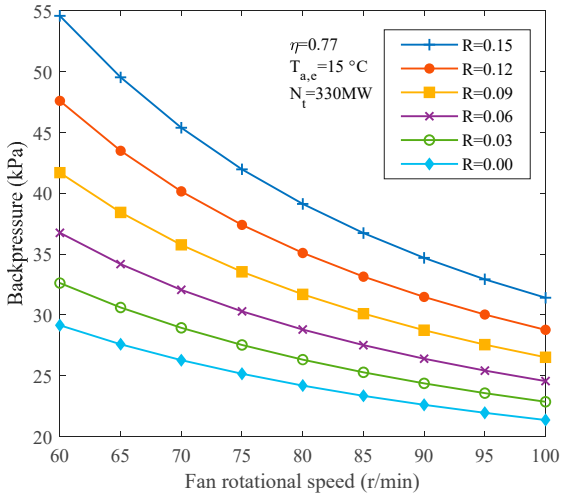

Figure 7. Backpressure at different fan speeds and plume recirculation rates.

In Figure 7, the condenser pressure increases with the plume recirculation rate. As the fan speed decreases, the influence of the change of the plume recirculation rate on the backpressure increases. The effect of plume recirculation on backpressure is similar to that of ambient temperature on backpressure, because plume recirculation causes an increase in fan inlet temperature. Compared with the design operating point of the condenser (R = 1, and n = 100 r/min), when the plume recirculation rate of the fan rose to 0.15, the backpressure increased by 10 kPa.

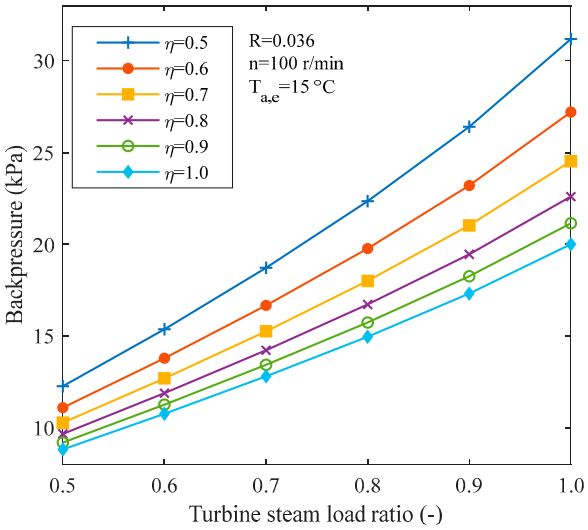

Figure 8. Backpressure at different load ratios and fan volumetric effectiveness.

In Figure 8, the condenser pressure increases as the fan volumetric efficiency decreases. When the turbine steam load ratio increases, the effect of fan volumetric effectiveness on backpressure increases. The fan face velocity is decreased under the disturbance of ambient wind, which is similar to the effect of fan speed reduction on backpressure. Compared with the design operating point of the condenser (η = 1, and N_T = 330 MW), when the volumetric effectiveness decreased by 0.5, the backpressure rose by 11 kPa.

3. Optimum backpressure

The optimum backpressure under different fan volumetric effectiveness and plume recirculation rates were calculated according to Equation (24) and are shown in Figure 9, when $T_{a,e}$ = 15 °C and N_T = 231 MW. The optimal backpressure decreases as the volumetric effectiveness increases, and decreases as the plume recirculation rate decreases. Compared with the design operation point of the condenser (η = 1, and R = 0), when η = 0.5 and R = 0.15, the optimum backpressure of the condenser increased by nearly 15 kPa.

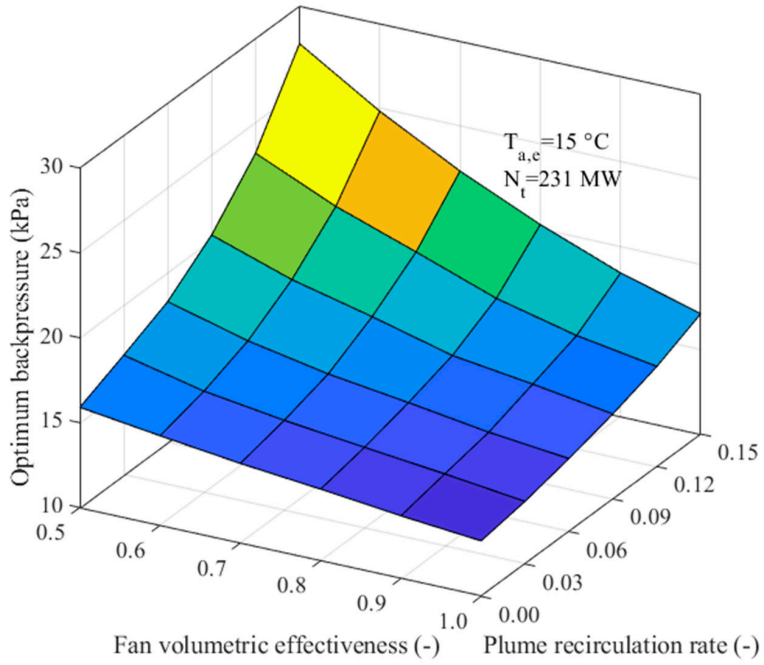

Figure 9. Optimum backpressure at different plume recirculation rates and fan volumetric effectiveness.

It was found that under different operating conditions, the fan volumetric effectiveness and plume recirculation rate have a significant impact on backpressure, which further affects the economy of the power plant. The performance explains why a sudden burst of ambient wind, especially from the direction of the boiler, can cause a rapid increase in the backpressure of the direct air-cooling power plant, resulting in an emergency shutdown.

4. Control Methodology

To overcome the negative effects of flow distortion or disturbances caused by ambient wind on the performance of the direct air-cooling condenser, a multi-model predictive control strategy was proposed to improve the control performance and economy.

4.1. Global Structure

The structure of the multi-model predictive controller for backpressure regulation is depicted in Figure 10. The difference between the output of each local model $y_m(k)$ and the output of the plant $y(k)$ is used to generate a model switching signal $\delta(k)$. The switching signal is sent to the model optimization and model prediction modules, respectively. The difference between the optimal set-point value generated by the optimization $r(k)$ and the predicted output of the selected model $y_p(k)$ is transmitted to the controller to calculate the control variable $u(k)$. Backpressure optimization is introduced in Section 3.2. The following sections present the local models, model prediction, control objective function, and switching rules.

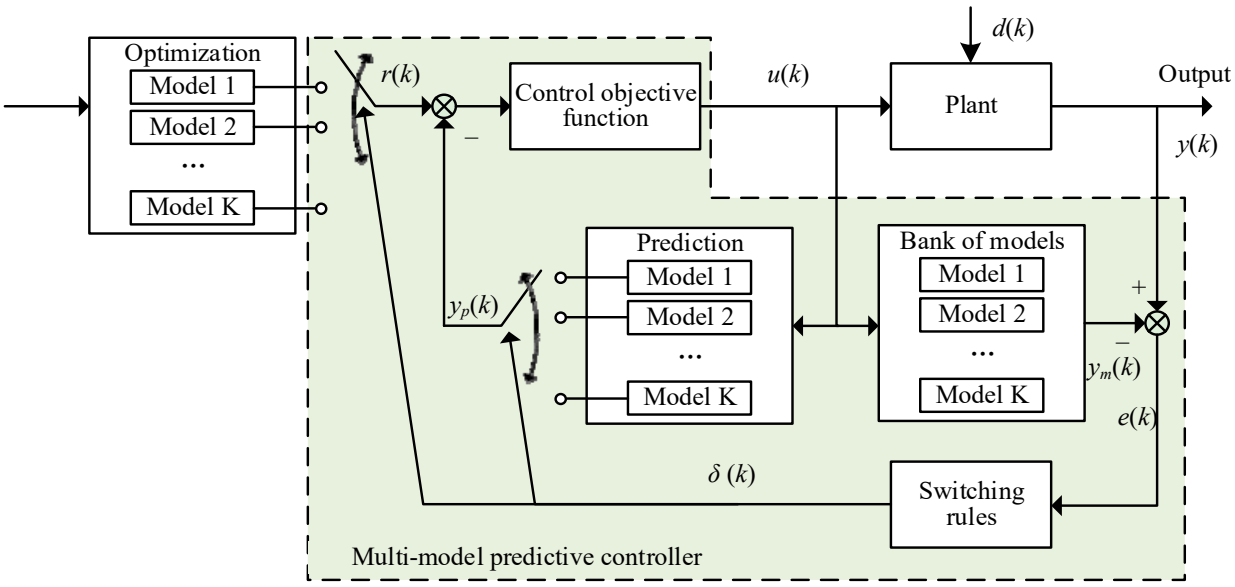

Figure 10. The structure of the multi-model predictive controller for the direct air-cooling condenser.

4.2. Bank of Local Model

At present, dozens of air-cooling units in the condenser are controlled as one unit, but the fans in different positions of the condenser have different performances under the ambient wind. Referring to the divisional control suggestions presented by previous studies [7,16–18], four division schemes were proposed for the direct air-cooling array according to the wind direction, as shown in Figure 11. The axial fans were divided into three groups according to the wind direction: windward fans, leeward fans, and other fans. Each group of fans was represented by an air-cooling unit model established in Equation (23) and adjusted separately. The average backpressure of all cooling units was taken as the direct air-cooling condenser backpressure.

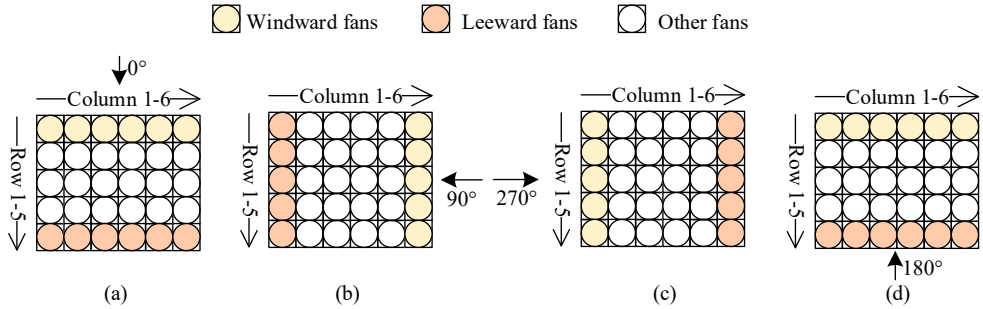

Figure 11. Schematic of divisional regulation of fan array under different wind directions: (**a**) in wind direction 0°; (**b**) in wind direction 90°; (**c**) in wind direction 270°; (**d**) in wind direction 180°.

When the wind direction is 90°, the influence of ambient wind on the airflow of the direct air-cooling condenser is axisymmetric with that of when the wind direction is 270°. Therefore, this paper shows the controller performance by switching between the three models in Figure 11a,c,d. When the ambient wind speed was 6 m/s, the plume recirculation rate and volumetric effectiveness were measured by field experiments and scaled-down model experiments, respectively. The establishment of the scaled-down fan array model and experiments are introduced in [20]. The parameters are shown in Table 2. The plume recirculation caused by ambient wind gradually decreased in the order of wind direction angles of 180°, 270°, and 0°. The plume recirculation rate and wind direction have a strong correlation at the same wind speed, and therefore, this characteristic is utilized in model switching.

Table 2. The Parameters of Local Models.

Wind Direction (°)	Average Plume Recirculation Rate (-)	Volumetric Effectiveness (-)		
		Windward Fans	Leeward Fans	Other Fans
0	0.036	0.55	0.85	0.78
270	0.06	0.5	0.97	0.79
180	0.15	0.55	0.85	0.78

4.3. Model Predictive Control

Model predictive control (MPC) is an effective, advanced control technique for constrained multiple-input multiple-output (MIMO) control problems in the process industry. The brief idea of MPC is as follows:

At every sampling instant k, a process model is used to predict the current and future values of the output variables with current measurements:

$$\begin{aligned} x(k+1) &= Ax(k) + Bu(k) \\ y(k) &= Cx(k) \end{aligned} \tag{26}$$

The future output can be estimated as:

$$y(k+P) = C\left(A^P x(k) + \sum_{j=0}^{P-1} A^j B u_{P-1-j}\right) \tag{27}$$

Let $y_P(k) = [y(k+1)^T, \cdots, y(k+P)^T]^T$ be the predicted values for the output and $u_M(k) = [u(k+1)^T, \cdots, u(k+M-1)^T]^T$ be the future manipulated input, where the subscripts P and M are the prediction and control horizon, respectively. The manipulated input is held constant after the M control moves.

The constraints on the input and output are:

$$\begin{array}{c} u_{\min} \le u_M(k) \le u_{\max} \\ y_{\min} \le y_P(k) \le y_{\max} \end{array} \tag{28}$$

where the subscripts min and max stand for lower and upper bounds, respectively.

The future manipulated variables are calculated by optimizing an objective function so that a sequence of predicted output reaches the set-point in an optimal manner:

$$\min J(k) = \|y_P(k) - r(k)\|^2_{Q_y} + \|\Delta u_M(k)\|^2_{Q_u} \tag{29}$$

where Q_y and Q_u are the symmetric positive definite weight matrixes, and $r(k)$ is the set-point generated by the optimization. With the receding horizon approach, although a set of manipulated input is calculated, only the first move is implemented. Then, a new sequence of control is calculated at the next sampling time, with new measurements.

4.4. Model Switching Rules

When the environment or operating conditions of the system change, it is expected that the controller can quickly switch to the local model that most fits the current system state. A function of error is used as a criterion to evaluate which local model is optimal [22]:

$$\delta(k) = \arg \min_{i \in 1,2,\ldots,K} e_i^2(k) + \int_0^k e^{-\lambda(k-t)} e_i^2(t) dt \tag{30}$$

where $\delta(k)$ is the switch signal, $e_i(k) = y(k) - y_{m,i}(k)$ ($i = 1, \ldots, K$) is the ith model output error at time k, and λ is a forgetting factor. The criteria of local models are calculated at every sampling time, the local model with the smallest criterion is adopted as the best fit model, and the switch signal is sent to the optimization and model prediction modules. An appropriate forgetting factor is beneficial to avoid frequent switching. A forgetting factor with a small value can effectively avoid unnecessary switching, while a forgetting factor with a large value is conducive to the rapid response of the model.

4.5. Simulation Results and Discussion

When the ambient wind direction changed, the simulation results of the direct air-cooling condenser using the multi-model controller are as shown in Figure 12. The tracking performance of the multi-model predictive controller and the traditional predictive controller are compared.

The operating condition in t = 0 s was: N_T = 231 MW, $T_{a,e}$ = 15 °C, p = 13.5 kPa, n = 100 r/min, and R = 0.036. During the simulation: (1) At t = 0 s, the set-point of backpressure was increased to 14.4 kPa, which was the optimal backpressure. As the model fit the plant, there was no difference between the two controllers. (2) At t = 80 s, the plume recirculation rate increased from 0.036 to 0.15, resulting in an increment in condenser pressure, deviating from the set-point. With the proposed method, the prediction model was switched from model 1 to model 3, and the disturbance was quickly suppressed. (3) At t = 150 s, the set-point of backpressure was increased to 17.5 kPa, which was the optimal backpressure calculated according to model 3. The multi-model predictive controller acted rapidly to track the changed set-point, whereas the controller with a single prediction model experienced large overshoots and fluctuations, which were caused by the model mismatch. (4) At t = 300 s, the plume recirculation rate decreased to 0.1 There was no perfectly matching prediction model, but according to the switching rule, model 2 was the closest prediction model. The controller also provided a satisfactory effect. (5) At t = 400 s, the set-point of backpressure was decreased to 14.9 kPa, which was the optimal backpressure calculated according to model 2.

It can also be seen that while the divisional regulation of fans was adopted, the operating speeds of the three groups of fans were different, because the volumetric effectiveness

of the fans was reflected in the models. When the backpressure set-point value was high, the rotation speed of the windward fan and the leeward fan was relatively large, which was the expected control result.

In general, the proposed multi-model predictive control strategy for the direct air-cooling condenser has satisfactory control performance, can quickly switch the prediction model, and provide the optimal backpressure reference value according to the prediction model.

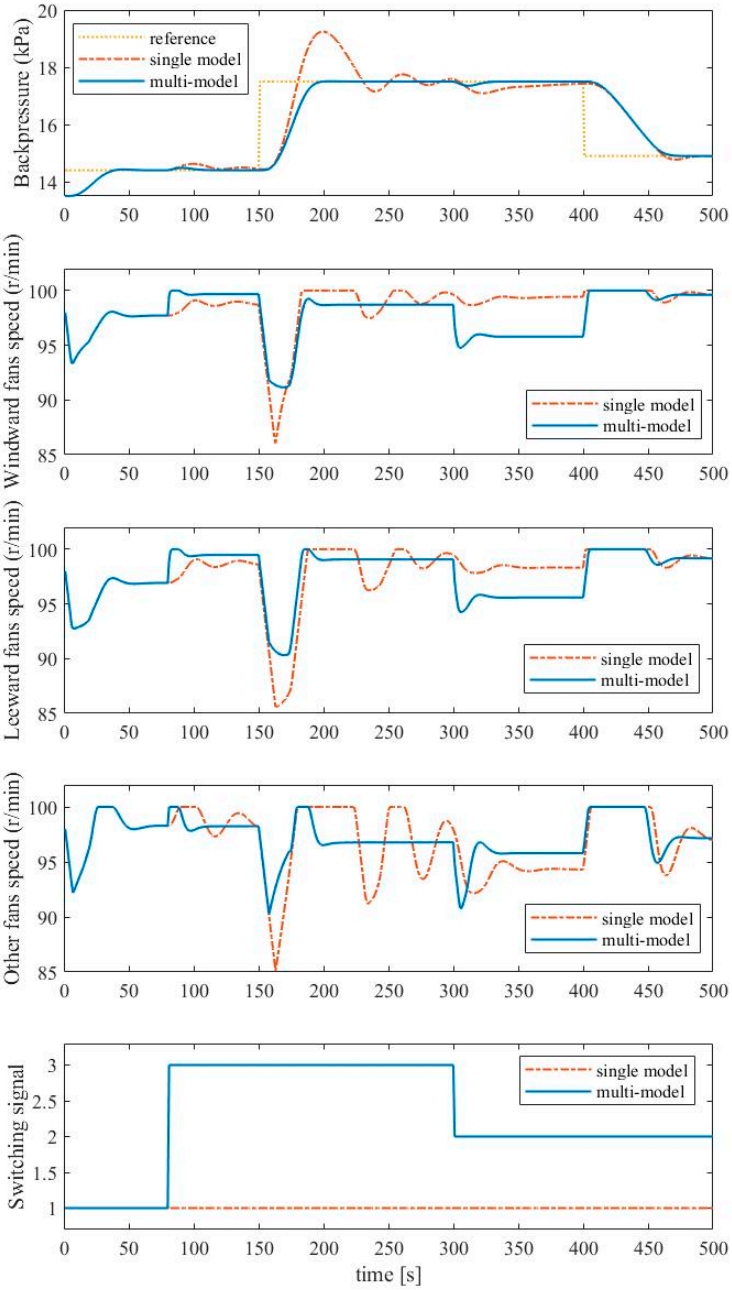

Figure 12. Tracking performance of the multi-model predictive controller.

5. Conclusions

A control-oriented direct air-cooling condenser model was established considering the fan volumetric effectiveness and the plume recirculation rate. The following conclusions were drawn:

(1) The model shows the influence of fan volumetric effectiveness and plume recirculation on the dynamic response and steady state of backpressure under various operating conditions.

(2) According to the wind direction, the fan array is divided into three groups: windward fans, leeward fans, and other fans, which are adjusted separately. At a certain wind speed, there is a strong correlation between wind direction and plume recirculation rate, and this relationship is utilized in model switching.

(3) A multi-model-based predictive control strategy for the direct air-cooling condenser is proposed. The analysis shows that applying the control strategy improves the robustness and performance of the system.

Author Contributions: Z.L.: conceptualization, methodology, investigation, simulation, and writing—original draft; Q.Y.: resources, data curation, formal analysis, and writing—review and editing. All authors have read and agreed to the published version of the manuscript.

Funding: This research was funded by the National Natural Science Foundation of China, grant number 51821004.

Conflicts of Interest: The authors declare no conflict of interest.

Appendix A

This section provides elements in matrix D of Equation (22) and matrix A and B of Equation (23). The thermodynamic properties and partial derivatives of steam and water can be calculated by a library based on the IAPWS IF-97.

$$D = \begin{bmatrix} d_{11} & d_{12} & 0 & 0 \\ d_{21} & d_{22} & 0 & 0 \\ 0 & 0 & 0 & d_{34} \\ d_{41} & d_{42} & d_{43} & 0 \end{bmatrix} \tag{A1}$$

$$d_{11} = A_s L\left(\frac{d\rho_l}{dp}(1-\bar{\gamma}) + \frac{d\rho_g}{dp}\bar{\gamma}\right) \tag{A2}$$

$$d_{12} = A_s L(\rho_g - \rho_l) \tag{A3}$$

$$d_{21} = A_s L\left[\frac{d\rho_l h_l}{dp}(1-\bar{\gamma}) + \frac{d\rho_g h_g}{dp}\bar{\gamma} - 1\right] \tag{A4}$$

$$d_{22} = A_s L(\rho_g h_g - \rho_l h_l) \tag{A5}$$

$$d_{34} = C_w m_w \tag{A6}$$

$$d_{41} = \left(\frac{\partial\bar{\gamma}}{\partial p} + \frac{\partial\bar{\gamma}}{\partial x_{in}}\frac{\partial x_{in}}{\partial p} + \frac{\partial\bar{\gamma}}{\partial x_{out}}\frac{\partial x_{out}}{\partial p}\right) \tag{A7}$$

$$\frac{\partial\bar{\gamma}}{\partial p} = \frac{\partial\bar{\gamma}}{\partial c}\frac{dc}{dp} \tag{A8}$$

$$\begin{aligned}\frac{\partial\bar{\gamma}}{\partial c} = {} & \frac{1}{x_{out}-x_{in}}\left(\frac{1}{(1-c)^2} - \frac{2c}{(c-1)^3}\right) ln\left[\frac{x_{in}(c-1)-c}{x_{out}(c-1)-c}\right] \\ & + \frac{c}{(x_{out}-x_{in})(c-1)^2}\left[\frac{x_{in}-1}{x_{in}(c-1)-c} - \frac{x_{out}-1}{x_{out}(c-1)-c}\right] + \frac{1}{(c-1)^2}\end{aligned} \tag{A9}$$

$$\frac{dc}{dp} = \frac{2}{3}\left(\frac{\rho_g}{\rho_l}\right)^{\frac{-1}{3}}\left(\frac{1}{\rho_l}\frac{d\rho_g}{dp} - \frac{\rho_g}{\rho_l^2}\frac{d\rho_l}{dp}\right) \tag{A10}$$

$$\begin{aligned}\frac{\partial\bar{\gamma}}{\partial x_{in}} = {} & \frac{c}{(x_{out}-x_{in})^2(c-1)^2} ln\left[\frac{x_{in}(c-1)-c}{x_{out}(c-1)-c}\right] \\ & + \frac{c}{(x_{out}-x_{in})(c-1)^2}\frac{c-1}{x_{in}(c-1)-c}\end{aligned} \tag{A11}$$

$$\frac{\partial \bar{\gamma}}{\partial x_{out}} = \frac{-c}{(x_{out}-x_{in})^2(c-1)^2} ln\left[\frac{x_{in}(c-1)-c}{x_{out}(c-1)-c}\right] - \frac{c}{(x_{tout}-x_{in})(c-1)^2}\frac{c-1}{x_{out}(c-1)-c} \tag{A12}$$

$$\frac{\partial x}{\partial p} = \frac{-1}{h_g - h_l}\left[(1-x)\frac{dh_l}{dp} + x\frac{dh_g}{dp}\right] \tag{A13}$$

$$d_{42} = -1 \tag{A14}$$

$$d_{43} = \frac{\partial \bar{\gamma}}{\partial x_{out}}\frac{\partial x_{out}}{\partial h_{out}} \tag{A15}$$

$$\frac{\partial x}{\partial h} = \frac{1}{h_g - h_l} \tag{A16}$$

$$A = \left[D|_{(x_0,u_0)}\right]^{-1}\frac{\partial f(x,u)}{\partial x}\bigg|_{(x_0,u_0)} \tag{A17}$$

$$\frac{\partial f(x,u)}{\partial x} = \begin{bmatrix} 0 & 0 & 0 & 0 \\ f_{x,21} & 0 & f_{x,23} & f_{x,24} \\ f_{x,31} & 0 & 0 & f_{x,34} \\ 0 & 0 & 0 & 0 \end{bmatrix} \tag{A18}$$

$$f_{x,21} = -\alpha_i A_i \frac{dT_r}{dp} \tag{A19}$$

$$f_{x,23} = -\dot{m}_{out} \tag{A20}$$

$$f_{x,24} = \alpha_i A_i \tag{A21}$$

$$f_{x,31} = \alpha_i A_i \frac{dT_r}{dp} \tag{A22}$$

$$f_{x,34} = -\alpha_i A_i - \alpha_o A_o + \alpha_o A_o \frac{\partial T_{a,in}}{\partial T_w} \tag{A23}$$

$$\frac{\partial T_{a,in}}{\partial T_w} = \frac{R\alpha_o A_o}{(1-R)C_{p,a}\rho_a v_F A_F + R\alpha_o A_o} \tag{A24}$$

$$B = \left[D|_{(x_0,u_0)}\right]^{-1}\frac{\partial f(x,u)}{\partial u}\bigg|_{(x_0,u_0)} \tag{A25}$$

$$\frac{\partial f(x,u)}{\partial u} = \begin{bmatrix} f_{u,11} & 0 & 0 & 0 \\ f_{u,21} & f_{u,22} & 0 & 0 \\ 0 & 0 & f_{u,33} & f_{u,34} \\ 0 & 0 & 0 & 0 \end{bmatrix} \tag{A26}$$

$$f_{u,11} = 1 \tag{A27}$$

$$f_{u,21} = h_{in} \tag{A28}$$

$$f_{u,22} = \dot{m}_{in} \tag{A29}$$

$$f_{u,33} = \alpha_o A_o \frac{\partial T_{a,in}}{\partial T_{a,e}} \tag{A30}$$

$$\frac{\partial T_{a,in}}{\partial T_{a,e}} = \frac{(1-R)C_{p,a}\rho_a v_F A_F}{(1-R)C_{p,a}\rho_a v_F A_F + R\alpha_o A_o} \tag{A31}$$

$$f_{u,34} = A_o\left[(T_{a,in} - T_w)\frac{\partial \alpha_o}{\partial v_F} + \alpha_o\left(\frac{\partial T_{a,in}}{\partial v_F} + \frac{\partial T_{a,in}}{\partial \alpha_o}\frac{\partial \alpha_o}{\partial v_F}\right)\right]\frac{\partial v_F}{\partial n} \tag{A32}$$

$$\frac{\partial T_{a,in}}{\partial \alpha_o} = \frac{R(1-R)A_o C_{p,a}\rho_a v_F A_F (T_w - T_{a,e})}{\left((1-R)C_{p,a}\rho_a v_F A_F + R\alpha_o A_o\right)^2} \tag{A33}$$

$$\frac{\partial T_{a,in}}{\partial v_F} = \frac{R(1-R)\alpha_o A_o C_{p,a}\rho_a A_F (T_{a,e} - T_w)}{\left((1-R)C_{p,a}\rho_a v_F A_F + R\alpha_o A_o\right)^2} \tag{A34}$$

$$\frac{\partial \alpha_o}{\partial v_F} = 0.6\alpha_{o,0}{v_{F,0}}^{-0.6}{v_F}^{-0.4} \tag{A35}$$

$$\frac{\partial v_F}{\partial n} = \frac{\eta_F v_{F,0}}{n_0} \tag{A36}$$

References

1. Huang, C.; Hou, H.; Hu, E.; Yu, G.; Peng, H.; Yang, Y.; Wang, L.; Zhao, J. Performance Maximization of a Solar Aided Power Generation (SAPG) Plant with a Direct Air-Cooled Condenser in Power-Boosting Mode. *Energy* **2019**, *175*, 891–899. [CrossRef]
2. Liu, J.; Hu, Y.; Zeng, D.; Wang, W. Optimization of an Air-Cooling System and Its Application to Grid Stability. *Appl. Therm. Eng.* **2013**, *61*, 206–212. [CrossRef]
3. Du, X.; Liu, L.; Xi, X.; Yang, L.; Yang, Y.; Liu, Z.; Zhang, X.; Yu, C.; Du, J. Back Pressure Prediction of the Direct Air Cooled Power Generating Unit Using the Artificial Neural Network Model. *Appl. Therm. Eng.* **2011**, *31*, 3009–3014. [CrossRef]
4. Marincowitz, F.S.; Owen, M.; Muiyser, J. Experimental Investigation of the Effect of Perimeter Windscreens on Air-Cooled Condenser Fan Performance. *Appl. Therm. Eng.* **2019**, *163*, 114395. [CrossRef]
5. Li, X.; Wang, N.; Wang, L.; Kantor, I.; Robineau, J.-L.; Yang, Y.; Maréchal, F. A Data-Driven Model for the Air-Cooling Condenser of Thermal Power Plants Based on Data Reconciliation and Support Vector Regression. *Appl. Therm. Eng.* **2018**, *129*, 1496–1507. [CrossRef]
6. Li, X.; Wang, N.; Wang, L.; Yang, Y.; Maréchal, F. Identification of Optimal Operating Strategy of Direct Air-Cooling Condenser for Rankine Cycle Based Power Plants. *Appl. Energy* **2018**, *209*, 153–166. [CrossRef]
7. He, W.F.; Chen, J.J.; Han, D.; Wen, T.; Luo, L.T.; Li, R.Y.; Zhong, W.C. Numerical Analysis from the Rotational Speed Regulation within the Fan Array on the Performance of an Air-Cooled Steam Condenser. *Appl. Therm. Eng.* **2019**, *153*, 352–360. [CrossRef]
8. Duvenhage, K.; Kröger, D.G. The Influence of Wind on the Performance of Forced Draught Air-Cooled Heat Exchangers. *J. Wind. Eng. Ind. Aerodyn.* **1996**, *62*, 259–277. [CrossRef]
9. Salta, C.A.; Kröger, D.G. Effect of Inlet Flow Distortions on Fan Performance in Forced Draught Air-Cooled Heat Exchangers. *Heat Recovery Syst. CHP* **1995**, *15*, 555–561. [CrossRef]
10. Fourie, N.; van der Spuy, S.J.; von Backström, T.W. Simulating the Effect of Wind on the Performance of Axial Flow Fans in Air-Cooled Steam Condenser Systems. *J. Therm. Sci. Eng. Appl.* **2015**, *7*, 21011. [CrossRef]
11. Yang, L.J.; Du, X.Z.; Zhang, H.; Yang, Y.P. Numerical Investigation on the Cluster Effect of an Array of Axial Flow Fans for Air-Cooled Condensers in a Power Plant. *Sci. Bull.* **2011**, *56*, 2272–2280. [CrossRef]
12. Louw, F.G. *Performance Trends of a Large Air-Cooled Steam Condenser during Windy Conditions*; Stellenbosch University: Stellenbosch, South Africa, 2011.
13. Guo, Y.; Zhang, D.; Wan, J.; Yu, D. Influence of Direct Air-Cooled Units on Primary Frequency Regulation in Power Systems. *IET Gener. Transm. Distrib.* **2017**, *11*, 4365–4372. [CrossRef]
14. Yang, T.; Wang, W.; Zeng, D.; Liu, J.; Cui, C. Closed-Loop Optimization Control on Fan Speed of Air-Cooled Steam Condenser Units for Energy Saving and Rapid Load Regulation. *Energy* **2017**, *135*, 394–404. [CrossRef]
15. Zhang, Y.; Zhang, F.; Shen, J. On the Dynamic Modeling and Control of the Cold-End System in a Direct Air-Cooling Generating Unit. *Appl. Therm. Eng.* **2019**, *151*, 373–384. [CrossRef]
16. Liu, L.; Du, X.; Xi, X.; Yang, L.; Yang, Y. Experimental Analysis of Parameter Influences on the Performances Ofdirect Air Cooled Power Generating Unit. *Energy* **2013**, *56*, 117–123. [CrossRef]
17. Li, J.; Bai, Y.; Li, B. Operation of Air Cooled Condensers for Optimised Back Pressure at Ambient Wind. *Appl. Therm. Eng.* **2018**, *128*, 1340–1350. [CrossRef]
18. Huang, W.; Chen, L.; Wang, W.; Yang, L.; Du, X. Cooling Performance Optimization of Direct Dry Cooling System Based on Partition Adjustment of Axial Flow Fans. *Energies* **2020**, *13*, 3179. [CrossRef]
19. Huang, W.; Chen, L.; Yang, L.; Du, X. Energy-Saving Strategies of Axial Flow Fans for Direct Dry Cooling System. *Energies* **2021**, *14*, 3176. [CrossRef]
20. Luo, Z.; Liu, J.; Huusom, J.K. Energy-Efficient Operation of a Direct Air-Cooled Condenser Based on Divisional Regulation. *Int. J. Refrig.* **2021**, *132*, 233–242. [CrossRef]
21. Qiao, H.; Laughman, C.R.; Aute, V.; Radermacher, R. An Advanced Switching Moving Boundary Heat Exchanger Model with Pressure Drop. *Int. J. Refrig.* **2016**, *65*, 154–171. [CrossRef]
22. Zhu, H.; Shen, J.; Lee, K.Y.; Sun, L. Multi-Model Based Predictive Sliding Mode Control for Bed Temperature Regulation in Circulating Fluidized Bed Boiler. *Control Eng. Pract.* **2020**, *101*, 104484. [CrossRef]